ORIGINAL ARTICLE

Investigation of a large collapse sinkhole affecting a multi-storey building by means of geophysics and the trenching technique (Zaragoza city, NE Spain)

F. Gutiérrez · J. P. Galve · P. Lucha · J. Bonachea · L. Jordá · R. Jordá

Abstract An active sinkhole around 100 m long has been investigated in the city of Zaragoza (NE Spain). Subsidence activity on this depression, including the sudden occurrence of a collapse sinkhole 5 m across, led to the abandonment of a factory in the 1990s. At the present time, a building with 100 flats and shallow pad foundations partially built on the sinkhole, is affected by rapid differential settlement. The development of the sinkhole results from the karstification of the halite- and glauberite- bearing bedrock and the sagging and collapse of the overlying bedrock and alluvium, more than 30 m thick. GPR and electrical resistivity profiles have provided information on the distribution and geometry of the subsidence structure. The application of the trenching technique and geochronological methods (AMS and OSL dating) has allowed us to infer objective and practical data on the sinkhole including (1) Limits of the subsidence structure, (2) subsidence mechanisms, (3) cumulative subsidence (>408 cm), (4) subsidence rates on specific failure planes (>1.8 cm/year), (5) episodic displacement regime of some fault planes. The available information indicates that the progressive deformation recorded in the building will continue and might be punctuated by events of more rapid displacement. This work illustrates the practicality of the trenching technique for the study of sinkholes in mantled karst areas.

F. Gutiérrez (✉) · J. P. Galve · P. Lucha · J. Bonachea
Edificio Geológicas, Universidad de Zaragoza,
C/. Pedro Cerbuna 12, 50009 Zaragoza, Spain
e-mail: fgutier@unizar.es

L. Jordá · R. Jordá
Rudnik Ingenieros Consultores, C/. Bustar 24,
28720 Bustarviejo, Madrid, Spain
e-mail: rudnikconsultores@hotmail.com

Introduction

Development projects in sinkhole-prone areas should be preceded by detailed investigations focussed on the identification of pre-existing sinkholes and subsurface features indicative of potentially unstable ground (cavities, irregular rockhead and subsidence structures). The avoidance of these areas is the safest and commonly most cost-effective sinkhole risk mitigation strategy (Cooper and Calow 1998; Gutiérrez et al. 2008b). However, in many cases owners, developers and planners, frequently with an inadequate perception of the risk, consider that sinkhole hazards do not justify building prohibition. When a building is constructed on a sinkhole or ground susceptible to subsidence, its design should include special foundations. These may distribute the load of the structures over large areas (shallow foundations) or transfer it to stable bedrock (e.g., piles) (Waltham et al. 2005). Frequently, the existence of active sinkholes and subsidence structures beneath buildings is detected by deformation of the structure after their construction. At this stage, the application of effective remedial measures may be very difficult, especially when the voids are located at considerable depth and cause rapid subsidence. Numerous examples illustrate that sinkholes may cause the collapse or demolition of buildings and even the loss of human lives when subsidence occurs in a catastrophic way (Table 1).

Some of the questions that need to be answered when a building is affected by an active sinkhole include: (1) What are the precise limits of the sinkhole and underlying subsidence structures; (2) How is the sinkhole going to behave

Table 1 Some examples of building destruction caused by sinkholes

Date and location	Geology	Sinkhole characteristics	Potencial triggers	Damage	References
1962 West Driefontein Mine (South Africa)	Dolomite aquifer more than 1 km thick	Bedrock collapse sinkhole 55 m across. Sudden occurrence	Dewatering by pumping for gold mining	Sinkhole engulfed a three-storey crusher plant with the loss of **29 lives**	Benzuidenhout and Enslin (1970) and De Bruyn and Bell (2001)
1964 Blyvoorruitzicht (South Africa)	Dolomite aquifer more than 1 km thick	Bedrock collapse sinkhole 55 m across. Sudden occurrence	Bedrock collapse sinkhole. Unkown size	Sinkhole engulfed 2 houses and part of other 2 with the loss of **5 lives**	Benzuidenhout and Enslin (1970) and De Bruyn and Bell (2001)
1970 Casetas (Spain)	Alluvium-covered salt-bearing evaporites	Cover and bedrock collapse sinkhole. 15 m across and 6.5 m deep	?	3 buildings demolished and 12 evacuated	Romana and Soriano (1971)
1970's Mosul (Irak)	Bare and interstratal gypsum karst	Bedrock and caprock collapse sinkholes	Artificial input of water to the ground?	Unkown number of buildings collapsed and damaged	Jassim et al. (1997)
1981 Winter Park, Florida (USA)	Mantled limestone karst	Cover collapse sinkhole. Sudden occurrence and rapid lateral growth	Water table lowering by pumping	Sinkhole engulfed 1 building, three cars and a swimming pool	Jammal (1984)
1988 Kuwait City (Kuwait)	Mantled carbonate karst	Three cover and bedrock collapse sinkholes up to 15 m across and 31 m deep	?	Evacuation of 133 houses	Goodings and Abdulla (2002)
1980–1985 Puilatos (Spain)	Alluvium mantled halite-bearing evaporites	Widespread subsidence	?	Abandonment and demolition of the totality of a village	Gutiérrez et al. (2008a)
1990's Dead Sea (Israel)	Soil mantled halite beds	Catastrophic cover collapse sinkholes up to several tens of metters in diameter	Human-induced lowering of the lake level	Destruction of storehouses and swallowing of 2 persons (rescued)	Frumkin and Raz (2001)
1994 Allentown, Pennsylvania (USA)	Mantled dolomitic limestone	2 cover collapse sinkholes 15–9 m across and 5–3 m deep	Leakages from water pipes?	Demolition of a seven-storey building. 6 million euros	Dougherty (2005)
1997 Ripon (UK)	Gypsum overlain by caprock and/or soil	Cover collapse sinkhole10 m across and 6 m deep. Rapid occurrence	?	4 garages destroyed. 1.5 million euros	Cooper and Waltham (1999)
1998 Oviedo (Spain)	Mantled cavernous gypsum	Catastrophic collapse sinkholes	Lowering of water table for excavation?	Demolition of one block with multi-storey buildings. 18 million euros	Gutiérrez et al., (2008a)
2003 Calatayud (Spain)	Alluvium mantled gypsum	Catastrophic cover collapse sinkhole 6 m across and 10 m deep	?	Demolition of a five storey building with 52 flats. 4.8 million euros	Gutiérrez et al. (2004, 2008a)

Human live lost in bold. Sinkhole description follows the classification of Gutiérrez et al. (2008c)

in the future; (3) Could the sinkhole undergo episodes of catastrophic subsidence. In addition to the frequently used investigation methods, the trenching technique, commonly applied in paleoseismological (McCalpin 1996) and land-slide investigations (e.g., Onida et al. 2001), may provide objective information on these practical issues (Gutiérrez et al. 2008b). The stratigraphy and deformation structures exposed in the trenches may allow us to infer and measure: (1) The limits of the ground affected by subsidence; (2) The subsidence mechanisms and magnitude (cumulative subsidence); and (3) The kinematics of the sinkhole in the past. Sinkhole fill deposits with cumulative wedge-outs record progressive deformation, whereas colluvial wedges, unconformities and truncated failure planes are indicative of rapid displacement events. Additionally, when numerical ages are obtained for key stratigraphic units, we may estimate subsidence rates, constrain the timing of subsidence events and correlate them with potential triggers like earthquakes or extreme hydrological events. To our knowledge, the trenching technique allied with geochronological methods has only been applied to one sinkhole in the outskirts of Zaragoza city (Gutiérrez et al. 2008d).

This paper analyses the interaction between a large sinkhole and a building with 100 flats in Zaragoza city (NE Spain), partially built upon an active subsidence structure. Additionally, this case study has been selected for testing the utility of the trenching technique in the investigation of sinkholes.

Geological and geomorphological setting

The studied sinkhole is located in the southwestern sector of Zaragoza city (Valdefierro suburb), at the southern margin of the Ebro River valley in NE Spain (Fig. 1). From the geological point of view, this area forms part of the central sector of the Ebro Tertiary Basin, which is the southern foreland basin of the Pyrenees. In the surroundings of Zaragoza city the sedimentary infill of the basin includes the subhorizontally lying evaporitic sequence of the Zaragoza Gypsum Formation (Quirantes 1978). According to oil exploration boreholes this formation locally reaches 800 m in thickness (Torrescusa and Klimowitz 1990). In outcrops, this Oligo-Miocene evaporitic succession exhibits 300 m of laminated and nodular secondary gypsum with interlayered marls and shales. In the subsurface the formation is primarily composed of anhydrite/gypsum, halite and glauberite (Salvany et al. 2007 and references therein). Most likely, previously existing halite and glauberite units have been removed by interstratal dissolution from the outcropping sequence (Gutiérrez et al. 2007; Guerrero et al. 2008). Due to their high solubility, the existence of halite and glauberite ($Na_2Ca[SO_4]_2$) in the bedrock is a crucial factor for the development of subsidence phenomena. Whereas the equilibrium solubility of gypsum at 25°C is 2.4 g/l, halite and glauberite solubilities reach 360 and 118 g/l, respectively (Ford and Williams 1989). The tertiary bedrock is affected by subvertical joints and small-throw normal faults with prevalent N–S, E–W, and NW–SE trends (Arlegui and Simón 2001). Locally, the evaporitic bedrock displays an intense and chaotic deformation (synforms, collapse structures, collapse breccias) related to subsidence phenomena caused by interstratal karstification processes (Gutierrez-Santolalla et al. 2005; Guerrero et al. 2004, 2008). These gravitational structures are particularly abundant in the areas where the evaporites are covered by Quaternary alluvium. In these mantled karst settings the alluvium is commonly underlain by a karstic residue made up of gray marls with gypsum fragments resulting from the dissolution of the bedrock. Generally, the variable thickness of this residual material is proportional to the amount of evaporites removed by karstification from the rockhead (Gutiérrez et al. 2008c).

A morphostratigraphic sequence of 11 terrace levels (T11: 210–200 m, T10: 180–190 m, T9: 150–160 m, T8: 120–130 m, T7: 100–105 m, T6: 85–90 m, T5: 65–70 m, T4: 40–55 m, T3: 25–35 m, T2: 10–15 m, T1: 2–7 m, above the current channel) has been mapped in this sector of the Ebro River valley (Guerrero et al. 2008). The sinkhole analysed in this paper is located in the terrace T4 of the Ebro River (Fig. 1) at 40 m above the present channel and at 237 m a.s.l. In this sector, the Quaternary alluvium underlying the T4 terrace surface has a variable thickness locally reaching more than 50 m. The anomalously high thickness of the fluvial deposits is related to synsedimentary subsidence phenomena caused by the karstification of the bedrock (Gutiérrez and Gutiérrez 1998; Benito et al. 1998, 2000; Guerrero et al. 2004, 2008). The T4 terrace of the Ebro River is correlative to the terrace level of the neighbouring Huerva River that shows the highest thickness (>60 m) and records the main period of synsedimentary karstic subsidence. The dissolution-induced subsidence that affects the Quaternary terraces in the Huerva valley is primarily related to the dissolution of halite and glauberite units (Guerrero et al. 2008). The log of a mining exploration borehole drilled around 7 km to the south of the studied sinkhole (Fig. 1, borehole A5) shows glauberite units and a halite unit more that 30 and 70 m thick, respectively. The elevation of the glauberite units overlap with that of the thickened alluvium in the studied location and the top of the halite unit is located at approximately the same elevation as the base of this alluvial deposit (Salvany et al. 2007). This lithostratigraphic information strongly suggests that the synsedimentary subsidence that affected the Ebro River in the analysed area was largely related to the karstification of highly soluble salts.

Fig. 1 Geographic location and photogeomorphological sketch of the sinkhole area. The sector covered by the geomorphological map is shown in the digital elevation model. In addition to the studied sinkhole, those marked Sx correspond to karstic depressions that have caused damage to buildings and factories. See text for explanation
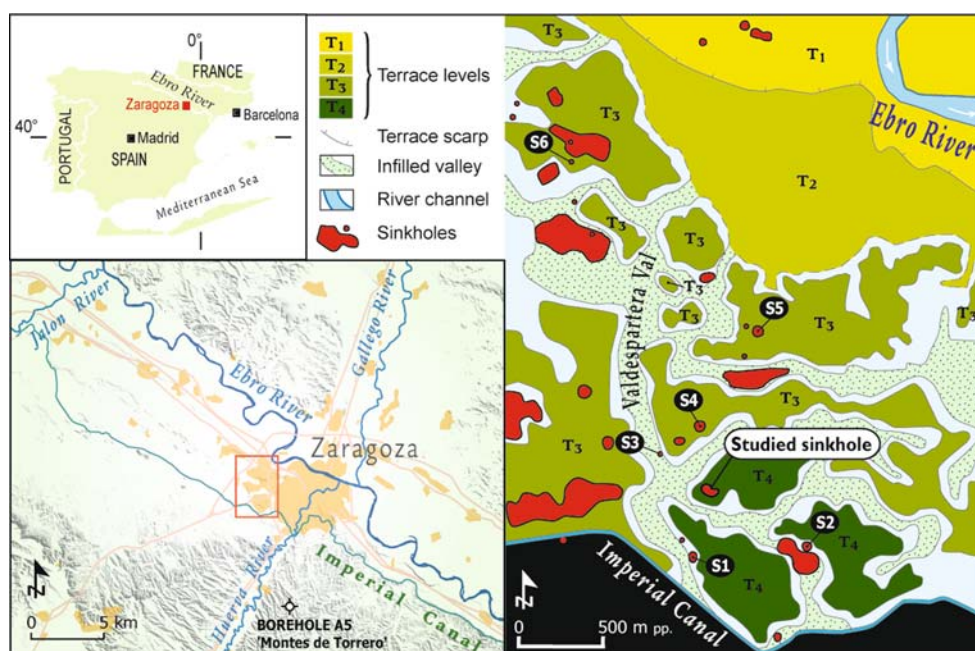
The geomorphological sketch presented in Fig. 1 shows that the terrace levels T4 and T3 are densely dissected by a system of flat-bottom infilled valleys with a dominant E-W trend that drain into the trunk Valdespartera Val, with a N–S orientation. The infilled valleys and the terraces T4 and T3 show a large number of sinkholes in the western sector of the mapped area. Some depressions have been captured by the drainage network and others create internally drained areas within infilled valleys disrupting the surface drainage. There seems to be two morphologic and genetic end-members in the sinkholes mapped in the area (Gutiérrez et al. 2008c): (1) Subcircular scarp-edged depressions commonly less than 100 m in diameter essentially generated by brittle deformation and collapse, most likely cover and bedrock collapse sinkholes. (2) Vaguely-edged depressions with irregular geometries in plan view and generally several hundred meters long. Ductile sagging or passive bending is most probably the dominant subsidence mechanism in these basins, which frequently host collapse sinkholes of the former type.

In recent decades, numerous sinkholes which are clearly identifiable on old aerial photographs (e.g., 1946, 1956) and detailed topographic maps (1935, 1971–1974) have been filled and used as sites for the construction of human structures including buildings, factories and communication routes (Soriano and Simón 2002; Guerrero et al. 2004; Gutiérrez et al. 2008d). Subsidence caused by the activity of these sinkholes, and to a lesser extent related to the compaction of the associated anthropogenic made ground, has resulted in severe damage to human structures, leading to the demolition of buildings in a significant number of cases. For example, within the area mapped in Fig. 1,

subsidence in sinkholes S1–S6 has caused damage to buildings (S1, S2, S5) and factories (S3, S4, S6). The apartments built on sinkhole S5 were recently demolished. Soriano and Simón (2002) used detailed topographic surveys and the cumulative deformation measured in structures of known age to estimate subsidence rates of the order of several cm/yr in backfilled sinkholes in this area. These rates may include both karstic subsidence and compaction of the anthropogenic fill. The sudden occurrence of collapse sinkholes in factories has also been documented. A spectacular example was the sinkhole formed in the Pikolín factory next to highway 232 on April 1999. The crater, 10 m in diameter and 6 m deep, formed in a catastrophic way severely deforming the walls and roof of the factory (Soriano and Simón 2002).

History of the sinkhole and surface investigation

The studied sinkhole is clearly recognisable in the aerial photographs taken in August 1956 reproduced at an approximate scale of 1:30,000 (Fig. 2a). The depression mapped with a stereoscope using these images shows an elongated geometry and a major axial length of approximately 90 m. The topographic basin hosts a scarp-edged depression around 60 m long in the western sector. The dark bottom of this nested collapse feature reveals the presence of abundant vegetation in the 1956 images. The eastern sector of the depression shows a smaller scarp and displays a general inclination towards the west.

In 1962 a factory was built on the eastern sector of the sinkhole (Fig. 2b). Soon after its construction, the portion
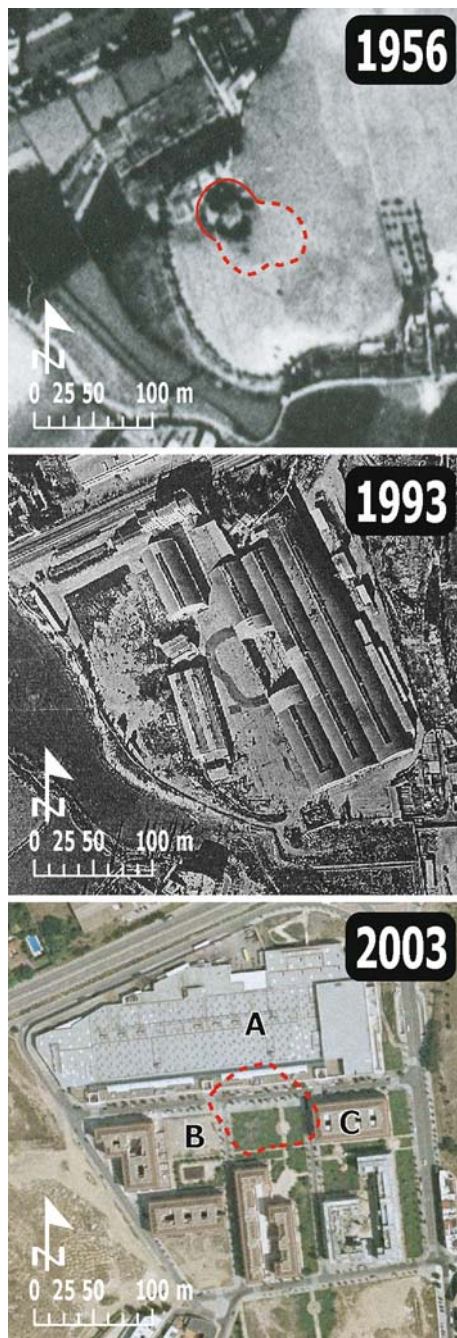
Fig. 2 Images of the sinkhole area taken on different dates. The edge mapped on the 1956 aerial photograph is based on stereoscopic interpretation. The 1993 image shows a dark band that defines the edge of the sinkhole and a gap in the demolished portion of a factory. The 2003 image shows the current urban distribution before the construction of building B. The sinkhole perimeter corresponds to that mapped by ENTECSA in 1996. The westernmost portion of building C is toppling towards the sinkhole

of the structure located on the sinkhole was affected by a progressive settlement and one night in 1985 a collapse around 5 m across and 3 m deep occurred on the floor of the factory (Mr. Carmelo Ayllón, pers. comm.). At the

beginning of the '80s, in order to stop the deformation of the structure and safeguard its integrity, several piles were driven into the Quaternary alluvium down to a depth of 18 m. These piles did not transfer the load to stable ground, and consequently the factory continued sinking. Subsequently, the part of the factory built on the sinkhole was demolished and in 1992 the facility was abandoned. An aerial photograph taken in 1993 shows a dark band defining the edge of the sinkhole and a gap in the factory coinciding with the sinkhole location (Fig. 2b).

In 1996, after the demolition of the previously mentioned factory, a company (ENTECSA) conducted a thorough geotechnical survey in the area for the construction of a department store (building A in Fig. 2c). This company produced a detailed map of the edge of the depression as defined by scarps and fissures. The sinkhole was also inventoried and mapped in a report on geological hazards (Simón et al. 1998), which was incorporated in the general land-use plan of the city and approved by the city council in 1999. The detailed map produced by ENTECSA has been georeferenced and superimposed on an orthophotograph taken in 2003 (Fig. 2c). This overlay shows that three buildings are partially underlain by the sinkhole. Building A, a large department store, was founded with piles locally more than 65 m deep reaching fresh bedrock and it has remained stable since its construction in 1997. One of the authors of this work (FG) examined the excavation cut in the terrace deposits for the construction of this structure. The excavation had an access ramp with a N145E orientation. The cuttings, up to 22 m high, showed a large basin structure with centripetal dips affected by synthetic and antithetic "normal faults" some of which reached the ground surface. A master failure plane juxtaposed terrace deposits against natural and anthropogenic deposits of the sinkhole fill.

Building B, whose NE corner was built with slab foundation, to date does not show any evidence of deformation in the façades (Fig. 3). Conversely, the western sector of building C has been affected by differential settlement. This building, with two basement floors and six storeys including the ground floor, hosts 100 flats. The value of this property has been estimated at 52 million Euros. The structure was founded with pads of reinforced concrete that transfer the load to the Quaternary alluvium. The pads are continuous beneath the walls of the structure (strips), and above the footings the structure is divided into five blocks separated by transverse dilation joints. The westernmost block of the building started to topple in January 2003 soon after the occupation of the building. The deformation is concentrated in the western joint resulting in its progressive widening upwards. In the upper part of the building, the toppling shows a main displacement component to the west and a minor component to the north. A
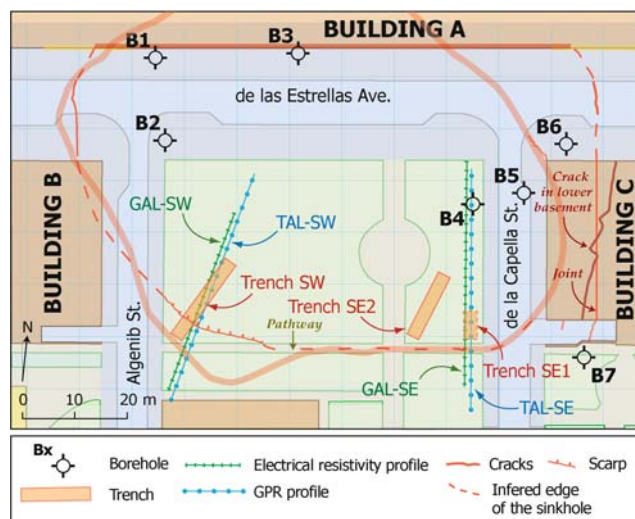
cumulative displacement of around 75 mm has been mea-
sured in the upper part of the joint on March 7, 2008
(Fig. 4a), yielding a mean deformation rate of 1.4 mm/year
for a time interval of 5.2 years (from January 2003). The
floor of the lower basement also shows a crack several
millimetres wide which intersects the western joint with a
NNE orientation (Fig. 3).

In August 2006 we produced a detailed map of the
sinkhole and related damage using a metric tape, a compass
and graph paper (Fig. 3). The southwestern marginal sector
of the sinkhole showed a scarp 15–20 cm high in the park
located between buildings B and C. Conversely, we were
not able to find any obvious deformation in the south-
eastern sector of the sinkhole. The area affected by active
subsidence next to the southern flank of building A was
clearly identified by means of cracks and tilting in the
pavement (Fig. 4b). Here, the settlement affects an area
larger than the perimeter mapped by ENTECSA in 1996,
which coincides with the crack that connects with the NW
corner of building C (Fig. 3). This indicates that since 1996
the sinkhole has enlarged in this sector. The vertical dis-
placement of around 30 cm measured in 2006 on the
sidewalk with respect to building A, constructed in 1997,
provides a subsidence rate of ca. 3 cm/year (Fig. 4b).

Subsurface investigation

Boreholes

The logs of a number of boreholes drilled within and
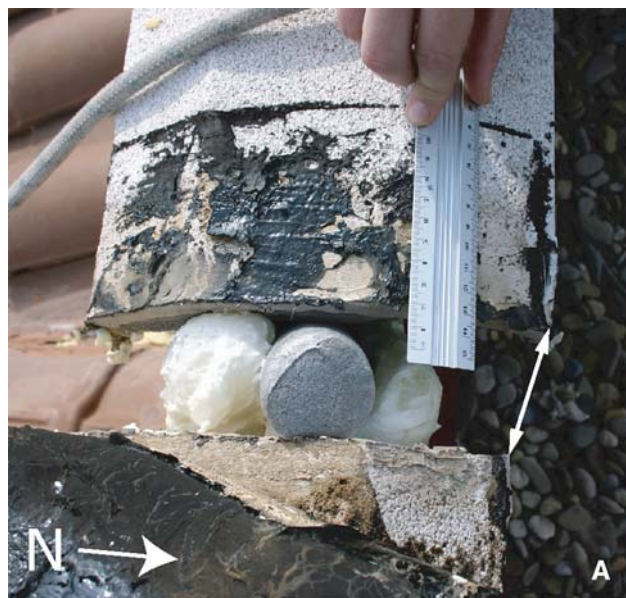around the perimeter of the sinkhole have been complied.

Fig. 4 a Opened joint in the upper part of the building showing a
main longitudinal displacement and a secondary transverse displace-
ment component (Photograph taken on March 7, 2008). **b** Tilting and
cracking caused by subsidence next to the stable building A
(Photograph taken on April 2007)

Three of them (B5–B7) reached fresh bedrock (Figs. 3 and
5). Four lithostratigraphical and geotechnical units can be
differentiated:

(a) Anthropogenic made ground and natural sinkhole fill
deposits. Although in the deepest sectors of the
sinkhole there must be a natural sinkhole fill deposit
beneath the made ground, the description of the logs
does not differentiate it. The thickness of this unit
increases towards the western sector of the sinkhole,
where the nested collapse depression recognised in

the 1956 images is located (Fig. 2a). Here, this unit is 6.3 and 5.7 m thick in boreholes B1 and B2 (Fig. 3). The anomalously high thickness found in borehole B4 (17.3 m) can be attributed to the backfilling of a ramp excavated for the construction of building A (Fig. 5).

(b) Fluvial terrace deposits. This unit consists of gravels with interbedded fine-grained facies (sands, silts and clay). The thickness of the fluvial sequence in the sinkhole area reaches 35 m in borehole B3 and the base of the unit descends from 28 to 37 m below the ground surface towards the western sector of the sinkhole (Fig. 5). A borehole drilled to the east of building C (not shown in the figures) penetrated 50 m of terrace deposits without reaching the base of the Quaternary cover. The drillers detected a void 1.95 m high partially filled with loose gravels at a depth of 13.15 m in borehole B3 (Fig. 5). This cavity located within the terrace deposits may be related to the upward propagation of a collapse chimney connected to dissolutional conduits at a greater depth.

(c) Dark gray clay with gypsum. This material corresponds to a karstic residue developed at the top of the evaporitic bedrock and/or to a strongly karstified collapse breccia generated by brittle deformation of rock cavity roofs. These highly porous breccias commonly act as zones of preferred groundwater circulation. Dissolution progressively transforms them from clast-supported packbreccias with voids into a karstic residue with bedrock relics (floatbreccias) (Warren 2006; Gutiérrez et al. 2008c). The thickness

of this unit ranges from 7 to more than 30 m. In boreholes B3 and B4 it exceeds 28.3 and 37.9 m and its base is located more than 65–71 m below the ground surface. In borehole B4 a total of 10.1 m of voids were detected between depths 45 and 62.8 m (Fig. 5). The anomalously high thickness of this unit in boreholes B3 and B4 indicates that it largely corresponds to a karstified breccia generated by the collapse of cavities developed within the bedrock.

(d) Gypsum bedrock. The top of the fresh bedrock, comprising gypsum beds with interbedded marls, has a very irregular geometry. It is located at around 37 m below the ground surface in boreholes B5–B7, whereas in boreholes B3 and B4, located a few meters to the west, it is situated at depths below 65 and 71 m, respectively. Additionally, boreholes B5 and B6 have penetrated cavities 0.5 and 1.6 m high within the bedrock (Fig. 5).

In June–August 2006 the water table was 37–37.5 m below the surface (199–200 m.a.s.l.), this was slightly below the top of the bedrock in boreholes B5–B7 and within the karstic residue and karstified breccias in boreholes B3 and B4 (Fig. 5). In the Ebro River valley, both the Quaternary alluvium and the karstic aquifer developed in the underlying evaporites are hydraulically connected. The hanging fluvial terraces act as recharge areas and the groundwater flowing through the alluvial and karstic aquifers discharges in the floodplain alluvium and in the Ebro River channel. Consequently, the materials situated

Fig. 5 Log of the boreholes drilled in the sinkhole area that reached fresh or karstified bedrock. Note the cumulative thickness of voids in borehole B4 and the large thickness of karstic residue in boreholes B3 and B4
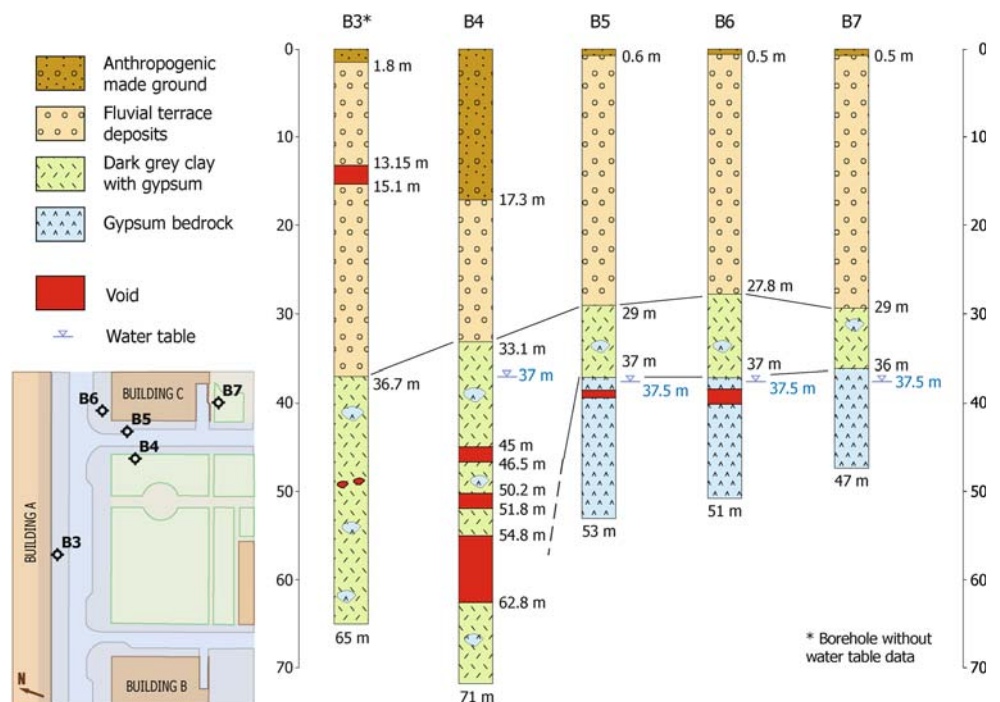
above the water table are dominated by downward vadose flows whereas the more saline groundwater in the phreatic zone flows slowly towards the bottom of the Ebro valley (Gutiérrez et al. 2007). The chemical analyses of two water samples with electrical conductivities of around 2,500 µS/cm collected in borehole B4 have been processed with Phreeqc Interactive 2.8 (Parkhurst and Appelo 1999), yielding negative gypsum and halite saturation indexes of 0.05–0.07 and 6.12–5.96, respectively. This means that the groundwater is within the equilibrium interval with respect to gypsum.

Geophysics

Eleven GPR profiles and three electrical resistivity profiles with a total length of 563 and 146 m, respectively, were conducted in the area enclosed by buildings A, B and C. The ground penetrating radar profiles were obtained using an IDS (Italy) georadar with an antenna of 400 MHz. The electrical resistivity surveys were carried out with an Iris Instruments equipment (Sycal Kid. Switch 24) using a dipole-dipole arrangement and a spacing of 2 m between electrodes. GRESWIN-IDS software was used to interpret the GPR profiles and the RES2Dinv software for the electrical imaging inversion. The working hypothesis was that these non-intrusive geophysical methods could allow

us to better identify the limits of the area underlain by the active subsidence structure and could also help us to locate the trenches at key sites avoiding major service mains. The most enlightening and representative profiles are presented in Figs. 6 and 7.

The GPR profile GAL-SW was conducted across the scarp in the southwestern sector of the sinkhole (Figs. 3 and 6). It shows reflectors truncated abruptly right beneath the scarp and tilted towards the central area of the sinkhole. Further investigation by a trench excavated roughly parallel to the GPR profile has revealed that the scarp is the geomorphic expression of a normal fault and a fissure resulting from the vertical displacement and rotation of the downthrown block. Additionally, the trench has allowed us to ascribe the offset and tilted contact of the GPR profile to the boundary between the top of the terrace deposit (clayey sands and silts) and a poorly-sorted and gravelly anthropogenic deposit (sinkhole fill) (Fig. 6). To the SW of the scarp, the GPR profile shows a pinch out associated to the base of the anthropogenic sinkhole fill. Here, the trench shows a terrace deposit tilted towards the sinkhole and extensional cracks This evidence indicates that in this sector the limit of the subsidence structure is located to the SW of the scarp. The scarp constitutes the manifestation of a major failure plane developed within the subsidence structure, but not its outer limit. This interpretation is in

Fig. 6 Correspondence between the GAL-SW georadar profile and the TAL-SW electrical resistivity profile with a simplified sketch of the log of the Trench SW
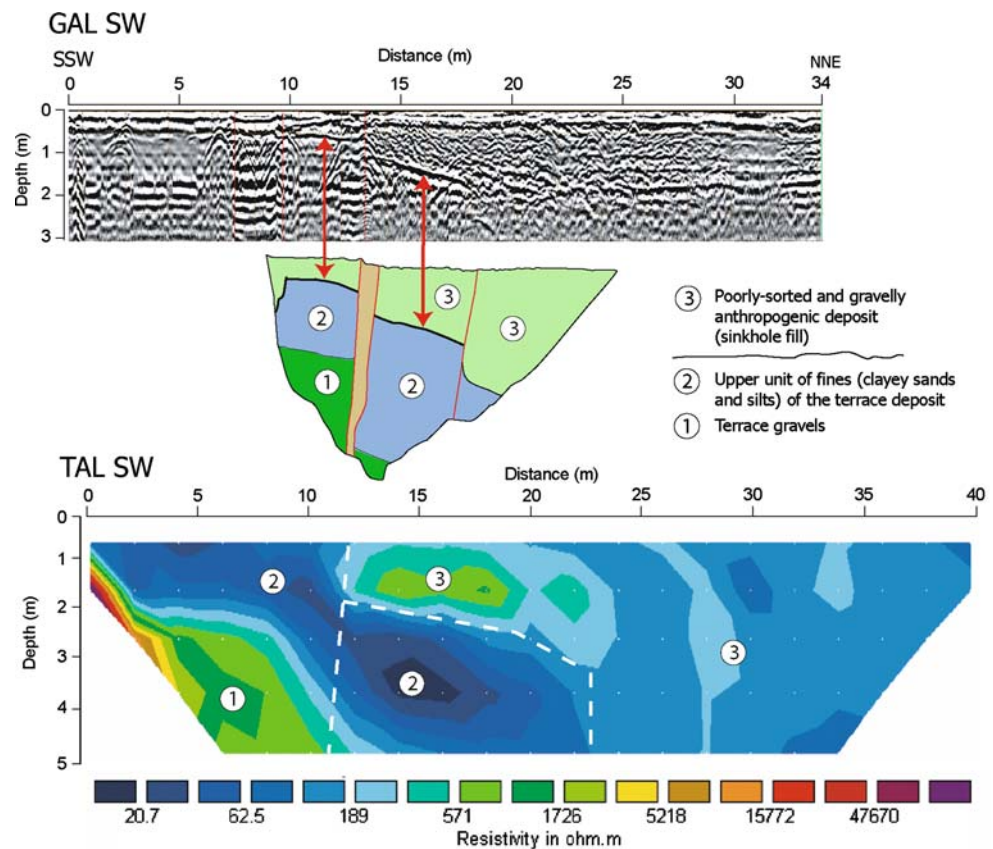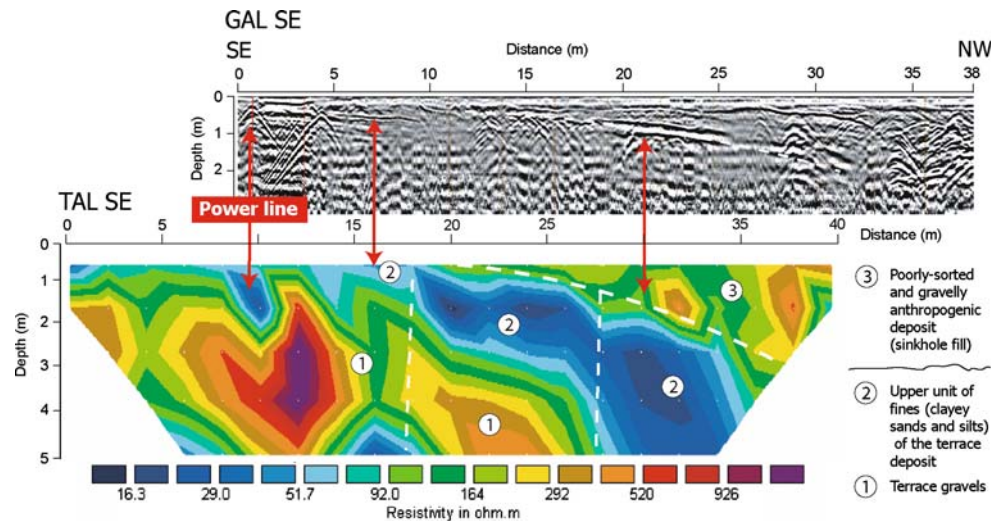
Fig. 7 Corrrespondence between the GPR profile GAL-SE and the electrical resistivity profile TAL-SW

agreement with the map produced by ENTECSA in 1996 (Fig. 3)

The trace of the electrical resistivity profile TAL-SW was largely coincident with that of the GPR profile GAL-SW (Figs. 3 and 6). Beneath the scarp this profile shows sharp lateral resistivity changes and a prominent step down to the NE in the base of a low resistivity material ascribable to the upper fine unit of the terrace deposit. The high resistivity unit overlying the fine terrace material in the downthrown block can be attributed to the gravely anthropogenic sinkhole fill. The high resistivity material underlying the fine terrace deposits in the upthrown block most likely corresponds to terrace gravels.

The GPR profile GAL-SE was gathered in the eastern-most sector of the park crossing a pathway about 15 m from the edge of building C (Figs. 3 and 7). This profile shows reflectors with a conspicuous dip to the north that reach the northern edge of the pathway. The trench dug next to this profile exposed a faulted terrace deposit dipping to the N made up of a lower gravel unit and an upper unit of fine material. This information has allowed us to ascribe the tilted reflectors of the GPR profile to the boundary between terrace gravels and fines. The electrical resistivity profile TAL-SE, which follows the same trace as the GPR profile (Fig. 3), shows a low resistivity unit with a down to the N step in the lower and upper boundaries. Similarly to the TAL-SW profile, the low resistivity material corresponds to the fines of the faulted terrace deposits and the overlying and underlying high resistivity materials to a gravelly anthropogenic fill and terrace gravels, respectively. Consistently with the GPR profile, the pinch out of the high resistivity material overlying the fine terrace deposits indicates that the subsidence structure reaches the northern edge of the pathway. According to the detailed map produced by ENTECSA in 1996, the limit of

the sinkhole in this sector roughly coincides with the pathway (Fig. 3).

Trenching

Trenching strategy and methodology

Initially we planned to dig two trenches the location of which was largely limited by the urban elements (Fig. 3). One of them was projected across the scarp with a NE–SW orientation in the southwestern sector of the sinkhole (Trench SW). The other one needed to be excavated with a N–S orientation in the eastern sector of the park as close to as possible to building C (Trench SE1). A limitation we faced was that the trenches should not affect the pathways of the park. Consequently we placed the southern edge of Trenches SW and SE1 next to the pathway (Figs. 3 and 8). This was a significant drawback since, according to the geophysical surveys and the map produced by ENTECSA in 1996, the edge of the sinkhole is located approximately beneath a path in the eastern sector of the park. The excavation of the Trench SE1 had to be stopped due to the instability of its walls, threatening the adjacent sidewalk. Therefore, we excavated Trench SE2 with an orientation oblique to that of the sinkhole edge; a position determined by the distribution of trees (Figs. 3 and 8). The trenches were excavated and filled with a backhoe. A reference grid with horizontal and vertical strings spaced 1 m apart was placed on the NE wall of Trench SW and on both walls of Trench SE2. The trench faces with reference grid were logged with graph paper (Figs. 9 and 10). Charcoal fragments and samples of fine-grained fluvial facies were collected for AMS dating (Poznań Radicarbon Laboratory) and OSL dating (Laboratorio de Datación y Radioquímica, Universidad Autónoma de Madrid), respectively.

Fig. 8 a View of trench SW. *Arrow* points to the scarp affecting the recent artificial soil. **b** View of trench SE2. **c** Open cracks in the SE wall of Trench SW, next to its southwestern edge. Images taken on January 2008

Trench SW

This trench, with a N24E orientation, was 16 m long, 4.9 m deep and around 2.5 m wide. Four types of deposits were mapped in the NE wall of this trench (Fig. 9):

(1) The oldest sediments correspond to terrace deposits composed of a lower gravel unit (TL) more than 2 m thick and an upper unit 3.5 m thick consisting of tabular beds of silty and clayey sand with interlayered tabular and lenticular beds or rounded pebble and granule gravel (TU). A total of seven subunits (TU1–TU7) have been differentiated in the upper terrace unit. Samples collected in subunits TU3 and TU5 have yielded OSL ages of 34,047 ± 2,966 and 23,685 ± 1,896 years BP, respectively (error margins at 1σ).

(2) Two different units of anthropogenic deposits (A1 and A2) made up of loose and chaotic gravels with brick and asphalt fragments. It is not clear whether the wedge-shaped base of unit A1 at the SW edge of the trench corresponds to an excavation, a fissure fill, or both. Northeast of fault F1 these units show a crude planar cross stratification dipping towards the central sector of the sinkhole that represent avalanche faces of the dumped material. This sector of the sinkhole does not show any evidence of anthropogenic fill in the 1956 images. Consequently, that date provide a minimum age for these units (less than 52 years old in 2008)

(3) A fissure fill 85 cm wide associated with fault F1 mainly consisting of loose gravels with brick and glass fragments and locally showing reoriented fabrics sub-parallel to the fissure walls. We have been able to identify two units in this fissure. The older unit (C1) is more consolidated and includes blocks of fine-terrace material derived from the walls of the fissure. The younger unit (C2) partially overlaps unit C1 and has large hollows and inter-granular voids. These fissures fill units cross-cut unit A1 and are truncated by the overlying soil (unit S).

(4) The anthropogenic deposits (A1 and A2) and the fissure fill (C1 and C2) are covered by an artificial soil 10–25 cm thick. The park and this soil must be younger than building A constructed in 1997.

Both the NE-tilted terrace sediments (TL and TU) and the anthropogenic deposits (A1 and A2) are offset by faults F1 and F2. Fault F2 constitutes an antithetic plane that dips 75° to the SW. Most likely it originally had a higher dip and has been rotated towards the centre of the sinkhole due to the tilting related to the opening of the fissure associated with fault F1. In fact, the terrace deposits in the upthrown and downthrown blocks of fault F2 dip around 10 and 14° to the NE. Fault F2 shows discontinuous lenticular shear zones 10–15 cm wide and the terrace sediments in the downthrown block are affected by an obvious drag fold. Fault F2 has vertically offset the base of the older anthropogenic deposit (A1) by 55 cm and is truncated by

Fig. 9 Orthorectified photomosaic and log of the Trench SW

TRENCH SW   Orientation: N24E   NW wall
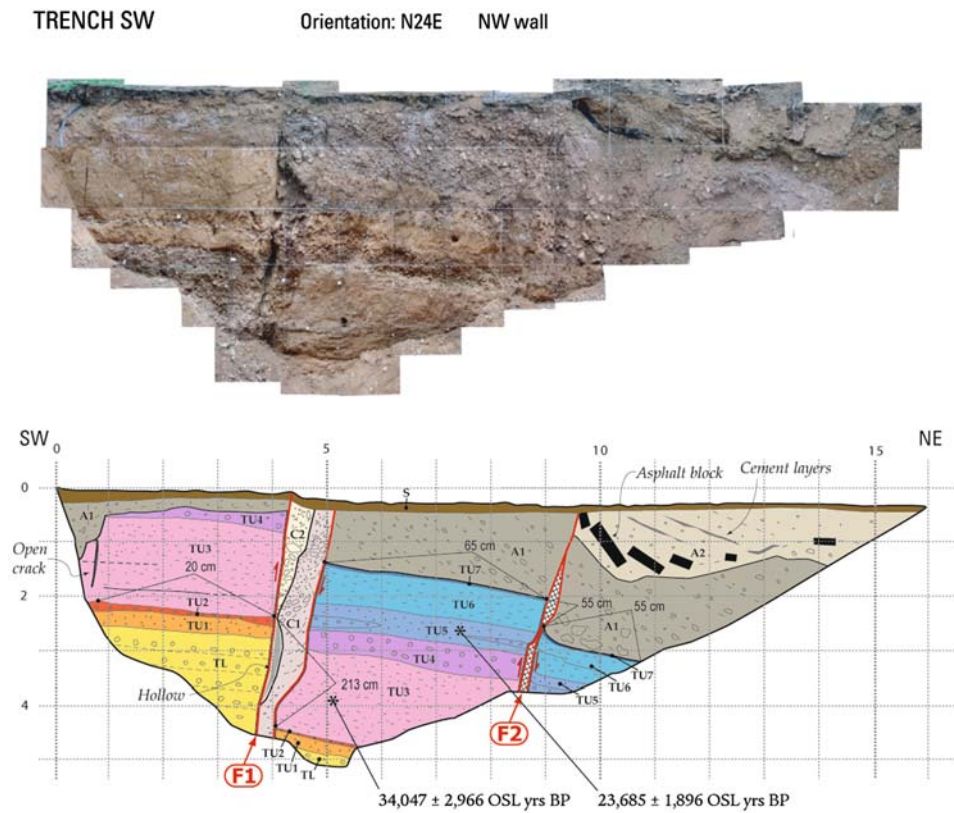
STRATIGRAPHIC UNITS

Terrace deposits

TU7	Light brown fine-grained sand
TU6	Brown massive clayey silt with abundant bioturbation and secondary carbonate.
TU5	Brown massive silty sand with scattered granules and lenticular beds of rounded gravel
TU4	Massive and rounded pebble gravel
TU3	Massive reddish brown silty sand with trace of root bioturbation with secondary carbonate. Fining upward sequence
TU2	Massive rounded pebble and granule gravel
TU1	Light brown massive silty sand
TL	Crudely bedded and rounded cobbly pebble gravel with imbricated fabrics (channel facies)

Unit TU

S	Grass-covered soil.

Fissure fills

C2	Very loose gravels with brick fragments with reoriented fabrics and with centimetre-scale voids.
C1	Loose gravels including brick and glass fragments with silty matrix and blocks of terrace fines (Tx)

Anthropogenic deposits

A2	Very loose gravel with large blocks of asphalt and concrete. Crudde planar cross bedding.
A1	Rounded gravel with sandy matrix and boulder NE of fault F2. Crude planar cross bedding

Symbols

• — 55 cm   Vertical distance between points   ⫽ Fault and shear zone

unit S. If we assume that unit A1 is less than 52 years old (post-1956) and unit S dates back to 1997, we can estimate a minimum vertical slip rate of ca. 1.3 cm/year on fault F2 (55 cm of displacement in less than 41 years). The geometrical relationships associated with fault F2 can be explained with just one event of 55 cm of vertical displacement that occurred between 1956 and 1997, after the deposition of unit A2 and before the installation of unit S. Another option, more probable in our opinion, is that fault F2 has undergone at least two episodes of displacement after the accumulation of unit A1 (post-1956) and before

unit S (1997) according to the following sequence of events. The first faulting event displaced unit A1 and created a depression on the downthrown block. This depression was filled by unit A2, which was subsequently displaced vertically by a minimum of 40 cm. However, the massive nature of the anthropogenic deposits does not allow us to ascertain if there is an angular unconformity between unit A1 and A2. Regardless of the actual number of faulting events, a relevant finding from the applied perspective is that failure planes in this sinkhole like F2 may have an episodic displacement regime.

Fault F1 is also an antithetic failure plane that dips 75–85° to the SW. Displacement on this extensional fault has vertical and horizontal components resulting in the foundering and tilting of the NE block towards the centre of the sinkhole and the creation of a fissure. This fissure is filled with two units of anthropogenic deposits (C1 and C2) and tapers downwards ranging from 85 to 25 cm wide in the trench wall. Although the fissure fill cross-cuts the artificial unit A1, this does not mean that the total horizontal separation on fault F1 (around 85 cm) has occurred after the accumulation of unit A1. The sharp contact between the fissure fills and unit A1 may be related to the settlement and downward migration of the fissure fill due to compaction and internal erosion processes. The terrace deposits have been offset vertically by 213 cm on fault F1. The base of unit A1 (post-1956 and pre-1997) shows a vertical separation of 95 cm, yielding a minimum vertical slip rate of 1.8 cm/year. Additionally, fault F1 has ruptured unit S creating a fresh scarp 15–20 cm high. Assuming that unit S dates from 1997, we can estimate a vertical slip rate of 1.4–1.8 cm/year on fault F1 from that date. The geometrical relationships do not allow us to infer the displacement regime of this fault, as either continuous, episodic or progressive punctuated by events of rapid slip.

The terrace deposits in the SW block of fault F1 dip around 4° to the NE and subunit TU3 is affected by prominent extensional cracks in which we were able to introduce our fingers (Fig. 8c). This evidence, in accordance with the information provided by the geophysical profiles GAL-SW and TAL-SW and the map produced by ENTECSA in 1996 (Figs. 3 and 6), indicates that the limit of the subsidence structure is located at an unknown distance to the SW of the scarp created by fault F1. For this reason, there may be failure planes with vertical displacement, but without geomorphic expression to the SW of the trench.

The deformation in the terrace deposits exposed in the trench records a cumulative vertical displacement of 408 cm. Vertical separation on faults F1 and F2 accounts for 268 cm (66%) of the total vertical displacement and the rest is caused by tilting (34%). Using this minimum cumulative subsidence of 408 cm and a maximum time interval of 23 kyr for this deformation, we can estimate a minimum long-term subsidence rate of 0.18 mm/year for the sinkhole. Obviously, the actual rate may be significantly higher since the sinkhole may be much younger than 24 ka and the total cumulative subsidence in the sinkhole higher than 408 cm. Unfortunately, the trench has not exposed natural sinkhole deposits whose numerical dating would allow us to obtain a tighter constraint for the time at which the sinkhole started to form in this sector. These deposits must be located in the central and deeper sector of the enclosed depression.

Trench SE2

This trench, with a N32E orientation, was 11.3 m long, 3.5 m deep and around 2.5 m wide. We mapped both walls of the trench since they showed different deformation structures. Figure 10 shows the log of the SE wall and the mirror image of a portion of the opposite wall. Three types of deposits have been differentiated:

(1) The oldest sediments are terrace deposits composed of two different units; a lower gravel unit 155 cm thick (TL) and an upper unit 235 cm thick of fine overbank material (TU). Two subunits have been differentiated in the upper tabular flood plain facies based on textural and colour changes (TU1 and TU2). Samples collected from the base and top of subunit TU1 have yielded OSL ages of $47,371 \pm 3,249$ and $36,549 \pm 2,813$ year BP (errors at 1σ). (2) Two units of anthropogenic deposits consisting of gravels with brick fragments, clayey sand matrix and chaotic fabrics. The older unit (A1) overlaps subunit TU2 and fills fissures on both walls of the trench. Two charcoal samples collected in the SE wall have provided AMS dates of 210 ± 30 and 150 ± 30 year BP (error at 1σ). These datings derived from an anthropogenic deposit must be considered as minimum ages. Consequently, the unit is younger than 1800 and probably was accumulated after 1956. The younger anthropogenic deposit (A2), up to 50 cm thick, truncates faults F1 and F2 in the NW wall and the fissure fill of the SE wall. It can be considered younger than 1956. (3) The unit A2 is covered by an artificial soil (S) up to 40 cm thick younger than 1997.

In the NW wall of the trench the terrace deposits are tilted 5–7° towards the central sector of the sinkhole and offset by two antithetic faults dipping 75° to the SW. Fault F1, with a N94E strike, offsets the terrace deposit by 67 cm vertically. This failure plane is truncated by unit A2 and consequently has been inactive at least since the accumulation of this anthropogenic deposit, probably younger than 1956. The tilting of the terrace deposits in the upthrown block of fault F1 suggests that there may be more failure planes to the SW of the trench. The geophysical profiles and the map produced by ENTECSA in 1996 indicate that the outer limit of the subsidence structure is located approximately beneath the path located to the SW of this trench (Figs. 3 and 7).

Fault F2 has vertically displaced the terrace deposits by around 43–55 cm. We have not been able to measure the strike of this plane. The slight tilting to the NE of the downthrown block has generated a fissure 5 cm wide filled with A1 deposits. Fault F1 affects unit A1 and is truncated by unit A2. Consequently, this structure has undergone at least one displacement event in historical times after the accumulation of unit A1 (probably post 1956) and before the accumulation of unit A2. These geometrical

Fig. 10 Orthorectified photomosaic and logs of the Trench SE2
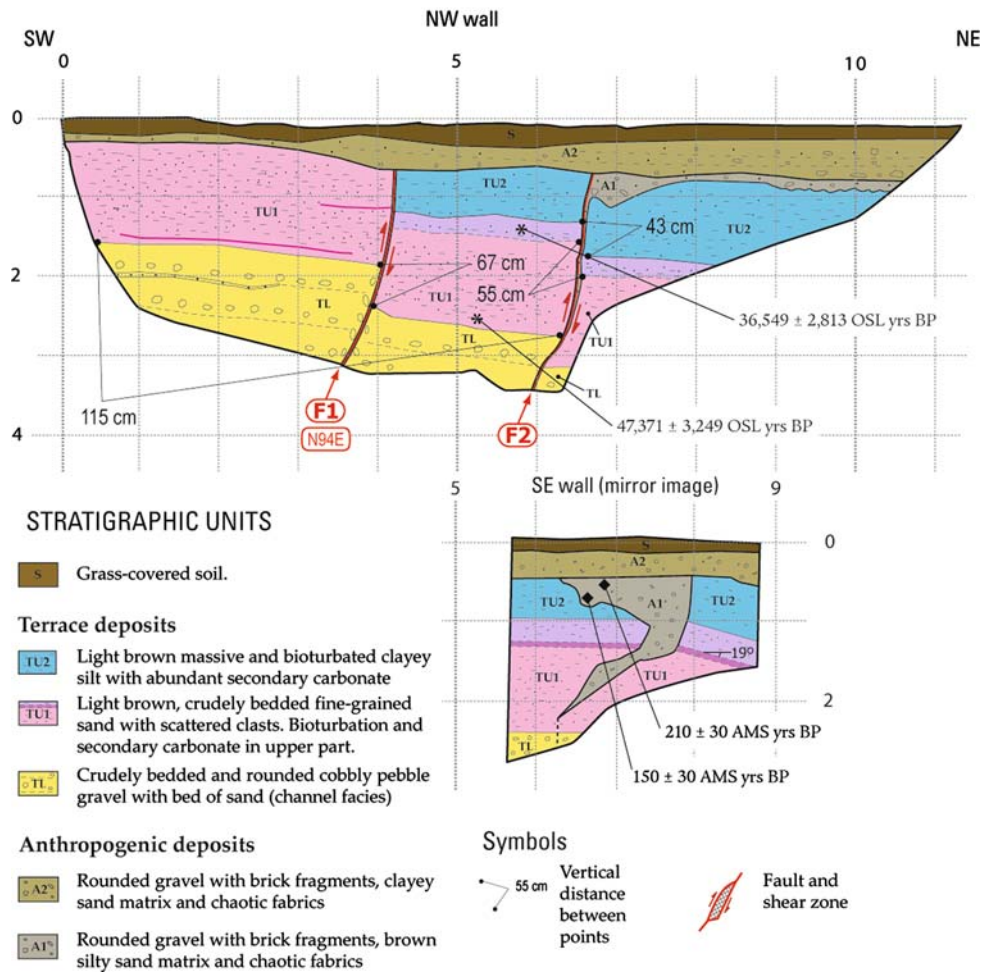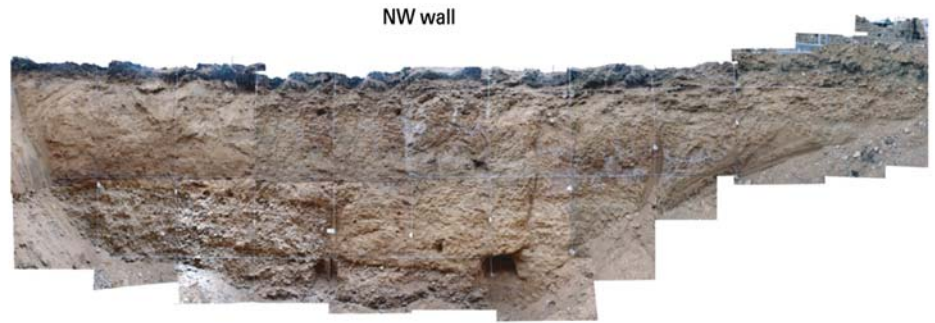
relationships and the available numerical ages suggest that fault F2 has moved in an episodic way in historical times.

Fault F2 of the NW wall has not been identified in the opposite side of the trench, which shows a fissure generated by the tilting of a block towards the central sector of the sinkhole. This fissure 10–15 cm wide, with sharp dip changes, has a N55E strike oblique with respect to the trench orientation (N32E). This is the reason why the fissure looks much wider in the log. The fissure is filled with unit A1 (post-1800 A.D.), indicating that at this point there was an open crack in historical times, most likely after 1956.

Discussion

The studied sinkhole has been developed on a terrace of the Ebro River whose deposits, locally more than 50 m thick,

have been affected by synsedimentary subsidence caused by the dissolution of the evaporitic bedrock. According to the available lithostratigraphical information, this subsidence coeval to the deposition of the terrace was primarily related to the interstratal karstification of glauberite and halite by upward phreatic flows (Guerrero et al. 2004, 2008). The sinkhole is around 100 m long and is clearly identifiable in aerial photographs taken in 1956. There is information on active subsidence in this sinkhole since the '60s. It led to the partial demolition and ultimately the abandonment of a factory in the '90s. The collapse 5 m across and 3 m deep that occurred in this factory in the '80s suggests that this depression might be locally affected by catastrophic subsidence events in the future. Subsequently, three buildings were constructed on this profusely studied sinkhole. One of these buildings with shallow pad foundations and partially located upon the sinkhole, has undergone a progressive toppling towards the sinkhole since its occupation in January 2003. An average horizontal displacement rate of 1.4 mm/year has been estimated for the upper part of the dilation joint in which deformation is concentrated. The comparison between a detailed map of the sinkhole produced in 1996 with the area currently affected by subsidence indicates that the sinkhole has enlarged in the area associated with the damaged building. The vertical displacement measured in some human structures at specific locations within the sinkhole has allowed us to estimate subsidence rates of 3 cm/year.

The maximum thickness of sinkhole fill deposits recorded in the boreholes indicates that the cumulative subsidence in the sinkhole may exceed 6 m. Assuming a mean depth of 3 m for the sinkhole and an area of 4,900 m^2, we can calculate a volume of 14,700 m^3 for the sinkhole. This rough estimate provides a minimum value for the volume of evaporites removed in solution, since collapse and brecciation processes entail a reduction in volume and large unfilled voids do exist beneath the sinkhole. The boreholes drilled in the sinkhole area indicate that the bedrock has undergone a significant differential karstification. The thickness of the karstic residue located between the alluvium and the fresh bedrock varies in a few meters form 7 to more than 30 m. Similarly, the depth of the top of the fresh bedrock (rockhead) changes from 37 to more than 71 m in a short distance. Voids with a cumulative height of 10.1 m have been identified between depths 45 and 62.8 m in a borehole drilled in the sinkhole.

The faulted basin structure exposed in an excavation carried out in the sinkhole during the '90s and the trenches dug for this work reveal that two main subsidence mechanisms are involved in the generation of the sinkhole: sagging (passive bending) and collapse (Gutiérrez et al. 2008c). The downward flexure of the alluvial cover is accompanied by the formation of steeply dipping or antithetic extensional faults. Vertical subsidence and tilting of the downthrown blocks result in the creation of scarps and fissures that taper downwards. Additionally, the tilting of the blocks implies the rotation and oversteepening of the failure planes towards the central area of the sinkhole. The extension accommodated by the formation of fissures may be explained by the shortening related to the passive sagging; the alluvial cover tends to occupy a progressively smaller area as it sags or bends passively. Moreover, bending creates an extensional regime in the outer zones of the basin structure contributing to the formation of normal faults (bending-moment faults). The ductile and brittle deformation in the alluvium is related to differential rockhead and/or interstratal karstification of the bedrock, probably involving halite and glauberite, and the breakdown of cavity roofs. Once the roof of a bedrock cavity has collapsed, subsidence may continue due to the karstification and compaction of the resulting highly porous collapse breccias. The collapse mechanism reflected by the normal faults is also substantiated by the presence of cavities in the subsurface and a karstic residue more than 30 m thick that very likely corresponds to a karstified collapse breccia.

The geophysical surveys have provided valuable information on the extent and geometry of the subsidence structure and the sinkhole. The GPR profiles provide an excellent image of the distribution and geometry of the deformation structures and sinkhole fill deposits located at shallow depth. The electrical resistivity profiles, although with a smaller resolution, have provided valuable information on the subsidence structure and distribution of the stratigraphic units at greater depths. A drawback of the non-intrusive geophysical methods is that there may be a significant uncertainty in the interpretations of their results. This limitation has been overcome supporting the geophysical interpretation by the excavation of trenches that provide 2D unambiguous information on the subsurface materials and the deformational structures.

Trench SW records a cumulative subsidence of 408 cm. Unfortunately, we have not been able to obtain a tight constraint for the age of the sinkhole, and consequently the estimated long-term subsidence rate (0.18 mm/year) using the youngest age of the terrace deposits (23 ka) must be considered as a minimum value, most probably considerably lower than the actual one. Minimum vertical slip rates of 1.8 cm/year (post-1956) have been calculated for the fault planes exposed in this trench. One of these faults offset an artificial deposit and is truncated by a younger one, suggesting an episodic displacement regime. Similarly, a fault in the Trench SE records at least one displacement event that occurred in historical times, most likely after 1956. This information on the kinematics of the failure planes indicates that the progressive deformation

recorded in the damage building could be punctuated by events of more rapid displacement in the near future.

The application of engineering corrective measures to the damaged building seems to be very difficult, given the large size of the sinkhole and specially the great depth at which the stable bedrock is located. However, some measures oriented to reduce the activity of the processes, like preventing irrigation and groundwater withdrawal, may help to slow down the subsidence process (Waltham et al. 2005; Gutiérrez et al. 2008b). The park located between buildings B and C was irrigated with water pumped from a well located next to building C. The input of water to the ground contributes to increase the load of the sediments located in the vadose zone, may reduce the mechanical strength of the soils and favour internal erosion and dissolution processes. The cones of depression generated by pumping involve an increase in the effective weight of the sediments and the replacement of slow phreatic flows by more rapid downward vadose flows that facilitate internal erosion processes.

Conclusions

In the case studied the subsidence damage is not related to the occurrence of a new sinkhole, but to the ongoing activity of a large, profusely studied and previously existing sinkhole. Perhaps surprisingly, this type of situation is relatively common in the surroundings of Zaragoza city. The risk could be reduced substantially and effectively by incorporating comprehensive sinkhole inventories and reliable sinkhole hazard maps in the land use planning process. Importantly, the elaboration and application of specific regulations for sinkhole hazards, including building codes by the local administration could be very cost-effective and would help to avoid destruction of property and the loss of human lives (LaMoreaux et al. 1997; Van Schalkwyk 1996; Paukstys et al. 1999; Richardson 2003).

Two main subsidence mechanisms operate in the studied sinkhole, sagging and collapse through the development of steeply dipping extensional faults. Dip-slip displacement on the failure planes is accompanied by tilting of the downthrown blocks towards the central area of the sinkhole, resulting in the generation of scarps and open fissures. The subsidence is caused by differential karstification of the evaporitic bedrock and the collapse of cavity roofs. This sinkhole can be described as a cover and bedrock sagging-collapse sinkhole according the genetic classification proposed by Gutiérrez et al. (2008c).

Subsidence activity will continue in the future and several lines of evidence indicate that it might include episodes of rapid displacement. (1) A collapse sinkhole 5 m across and 3 m deep formed in the sinkhole in the '80s. (2) Borehole data reveal the existence of cavities in the alluvium, karstic residue and bedrock. (3) One borehole penetrated voids with a cumulative height of 10.1 m. (4) The geometrical relationships associated with some failure planes exposed in the trenches are indicative of episodic displacement rather than continuous creep deformation.

Particular sinkholes are commonly investigated by means of boreholes and geophysical surveys. Boreholes provide objective information on the ground, but are limited to specific points (1D). Due to the complex nature of karst terrains the correlation and interpretation of borehole data may have a high degree of uncertainty. The geophysical techniques allow the ground to be explored in a non-intrusive way, but the interpretations may have a limited reliability. The inexpensive trenching investigation presented in this work demonstrates that it may provide a great deal of useful information on sinkholes and may help in the geophysical interpretations. The trenches offer the possibility of obtaining 2D and 3D objective information allowing us to locate the limits of the subsidence structures, interpret the subsidence mechanisms, measure cumulative subsidence values, and infer the displacement regime of subsidence structures (continuous, episodic or a combination of both). Additionally, the absolute dating of key stratigraphic units may allow us to constrain the timing of the sinkhole or subsidence events and estimate subsidence rates. Although the subsidence rates derived from trenches have a much lower resolution than those obtained by geodetic surveys, they commonly cover much longer time spans, providing a different and, in some cases, a more representative temporal perspective. Some of the drawbacks of the trenching technique include depth limitations, safety problems due to unstable walls and the need to disturb the ground.

References

Arlegui LE, Simón JL (2001) Geometry and distribution of regional joint sets in a non homogeneous stress field: case study in the Ebro Basin (Spain). J Struct Geol 23:297–313

Benito G, Pérez-González A, Gutiérrez F, Machado MJ (1998) River response to quaternary subsidence due to evaporite solution (Gallego River, Ebro Basin, Spain). Geomorphology 22(3/4):243–263

Benito G, Gutiérrez F, Pérez-González A, Machado MJ (2000) Morpho-sedimentological features in quaternary fluvial systems affected by solution-induced subsidence in the Ebro Basin, NE Spain. Geomorphology 33:209–224

Benzuidenhout CA, Enslin JF (1970) Surface subsidence and sinkholes in the dolomitic areas of the Far West Rand, Transvaal, Republic of South Africa. Land Subsidence. Int Assoc Hydrol Sci Publ 89:482–495

Cooper AH, Calow RC (1998) Avoiding gypsum geohazards: Guidance for planning and construction. WC/98/5, British geological survey, Nottingham, UK. Available in: http://www.bgs.ac.uk/dfid-kar-geoscience/database/reports/colour/WC98005_COL.pdf

Cooper AH, Waltham AC (1999) Subsidence caused by gypsum dissolution at Ripon, North Yorkshire. Q J Eng Geol Hydrogeol 32(4):305–310

De Bruyn IA, Bell FG (2001) The occurrence of sinkholes and subsidence depressions in the far West Rand and Gauteng province, South Africa, and their engineering implications. Environ Eng Geosci 7(3):281–295

Dougherty P (2005) Sinkhole destruction of Corporate Plaza, Pennsylvania. In: Waltham T, Bell F, Culshaw M (eds) Sinkholes and subsidence. Springer, Chichester, pp 304–308

Ford DC, Williams P (1989) Karst geomorphology and hydrology. Unwin Hyman, London

Frumkin A, Raz E (2001) Collapse and subsidence associated with salt karstification along the Dead Sea. Carbonates Evaporites 16(2):117–130

Goodings DJ, Abdulla WA (2002) Stability charts for predicting sinkholes in weakly cemented sand over karst limestone. Eng Geol 65:179–184

Guerrero J, Gutiérrez F, Lucha P (2004) Paleosubsidence and active subsidence due to evaporite dissolution in the Zaragoza area (Huerva River valley, NE Spain): processes, spatial distribution and protection measures for transport routes. Eng Geol 72(3/4):309–329

Guerrero J, Gutierrez F, Lucha P (2008) The impact of halite dissolution subsidence on fluvial terrace development: the case study of the Huerva River in the Ebro Basin (NE Spain). Geomorphology 100:164–179

Gutierrez-Santolalla F, Gutiérrez-Elorza M, Marín C, Maldonado C, Younger PL (2005) Subsidence hazard avoidance based on geomorphological mapping: the case study of the Ebro River valley mantled karst (NE Spain). Env Geol 48:370–383

Gutiérrez F, Galve JP, Guerrero J, Lucha P, Cendrero A, Remondo J, Bonachea J, Gutiérrez M, Sánchez JA (2007) The origin, typology, spatial distribution and detrimental effects of the sinkholes developed in the alluvial evaporite karst of the Ebro River valley downstream of Zaragoza city (NE Spain). Earth Surf Proc Land 32(6):912–928

Gutiérrez F, Calaforra JM, Cardona F, Ortí F, Durán JJ, Garay P (2008a) Geological and environmental implications of evaporite karst in Spain. Env Geol 53:951–965

Gutiérrez F, Cooper AH, Johnson KS (2008b) Identification, prediction and mitigation of sinkhole hazards in evaporite karst areas. Env Geol 53:1007–1022

Gutiérrez F, Guerrero J, Lucha P (2008c) A genetic classification of sinkholes illustrated from the Ebro valley evaporite alluvial karst (NE Spain). Env Geol 53:993–1006

Gutiérrez F, Guerrero J, Lucha P (2008d) Quantitative sinkhole hazard assessment: a case study from the Ebro valley evaporite karst (NE Spain). Nat Hazards 45:211–233

Gutiérrez F, Lucha P, Guerrero J (2004) La dolina de colapso de la casa azul de Calatayud (noviembre 2003). Origen, efectos y pronóstico. In: Benito G, Díez-Herrero A (eds) Riesgos naturales y antrópicos en Geomorfología. VII Reunión Nacional de Geomorfología, Toledo, pp 477–488

Gutiérrez F, Gutiérrez M (1998) Geomorphology of the tertiary gypsum formations in the Ebro depression (Spain). Geoderma 87:1–29

Jammal SE (1984) Maturation of the Winter Park sinkhole. In: Beck BF (ed) Proceedings of the 1st multidisciplinary conference on sinkholes. AA Balkema, Orlando, pp 363–369

Jassim SZ, Jibril AS, Numan NMS (1997) Gypsum karstification in the middle miocene fatha formation, Mosul area, northern Iraq. Geomorphology 18:137–149

LaMoreaux PE, Powell WJ, LeGrand HE (1997) Environmental and legal aspects of karst areas. Env Geol 29(1):23–36

McCalpin JP (1996) Field techniques in paleoseismology. In: McCalpin JP (ed) Paleoseismology. Academic Press, San Diego, pp 33–83

Onida M, Galadini F, Forcella F (2001) Application of paleoseismo-logical techniques to the study of late pleistocene-holocene deep-seated gravitational movements at the Mortirolo Pass (central Alps, Italy). Neth J Geosci/Geologie en Mijnbouw 80:209–227

Parkhurst DL, Appelo CAJ (1999) User's guide to PHREEQC (version 2), a computer program for speciation, batch reaction, one-dimensional transport, and inverse geochemical calculations. Water Resour Res Investig Rep 99–4259:312

Paukstys B, Cooper AH, Arustiene J (1999) Planning for gypsum geohazards in Lithuania and England. Eng Geol 52(1–2):93–103

Quirantes J (1978) Estudio sedimentológico y estratigráfico del Terciario continental de los Monegros. Instituto Fernando el Católico, CSIC, Zaragoza

Richardson JJ (2003) Local land use regulation of karst in the United States. In: B.F. Beck (eds) Sinkholes and the engineering and environmental impacts of karst. ASCE Spec Publ 112:492–501

Romana M, Soriano A (1971) Algunos ejemplos de subsidencias en las cercanías de Zaragoza. Primer Congreso Hispano-Luso-Americano de Geología Económica, vol 1. Madrid y Lisboa, pp 183–196

Salvany JM, García-Veigas J, Ortí F (2007) Glauberite-halite association of the Zaragoza gypsum formation (Lower Miocene, Ebro Basin, NE Spain). Sedimentology 54:443–467

Simón JL, Martínez-Gil FJ, Soriano MA, Arlegui LE, Caballero J (1998) Plan general de ordenación urbana. Anejo 3. Estudios Geológicos-Geotécnicos., Ayuntamiento de Zaragoza. Available in: http://cmisapp.ayto-zaragoza.es/ciudad/urbanismo/planeamiento/pgouz/memoria.htm

Soriano MA, Simón JL (2002) Subsidence rates and urban damages in alluvial dolines of the Central Ebro basin (NE Spain). Env Geol 42:476–484

Torrescusa S, Klimowitz J (1990) Contribución al conocimiento de las evaporitas Miocenas (Fm. Zaragoza) de la Cuenca del Ebro. In: Ortí F, Salvany JM (eds) Formaciones evaporíticas de la Cuenca del Ebro cadenas periféricas y de la zona de Levante. Enresa, Barcelona, pp 120–123

Van Schalkwyk A (1996) Legal aspects of development on dolomite land in South Africa. Env Geol 36:167–169

Waltham T, Bell F, Culshaw M (2005) Sinkholes and subsidence: karst and cavernous rocks in engineering and construction. Springer, Chichester, p 382

Warren JK (2006) Evaporites: sediments, resources and hydrocarbons. Springer, Berlin